Open quantum system models for the spectral filtering of vibrational coherences in broadband 2D electronic spectroscopy.

Dale Green, Giovanni Bressan, Stephen R. Meech and Garth A. Jones

School of Chemistry, University of East Anglia, Norwich NR4 7TJ, U.K.

e-mail: Dale.Green@uea.ac.uk

Engineering and Physical Sciences Research Council

Introduction

Vibrational coherences in ultrafast 2D electronic spectroscopy (2DES) reveal the motion of nuclear wavepackets, with their intensities governed by the displacement of the electronic excited states with respect to the ground state equilibrium geometry.[1] Recent development of broadband 2DES experiments has enabled access to a greater range of coherences involving higher energy states, providing valuable details of the excited state structure of molecules.[2] Here, combining the equation of motion-phase matching approach for finite laser spectra with the hierarchical equations of motion to correctly account for dephasing and dissipation,[3] we model half-broadband and broadband 2DES of cresyl violet to demonstrate the impact of spectral filtering vs. the relative displacement of two excited states (S_1 and S_n) on the intensity distribution of peaks in the beating maps for two vibrational modes with frequencies 350 cm^{-1} and 585 cm^{-1}.

Open Quantum Systems

The Hamiltonian is split into the system (solute) and the interaction with its environment (solvent).

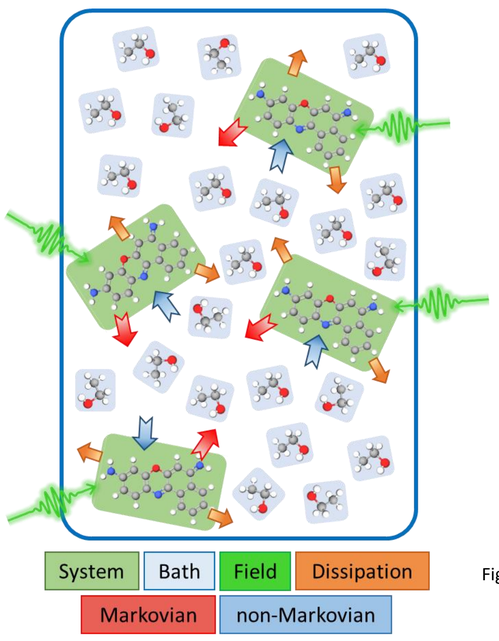

The 585 cm^{-1} and 350 cm^{-1} modes of cresyl violet are modelled as harmonic oscillators coupled to three electronic states, where the excited states S_1 and S_n are displaced along the vibrational coordinate with respect to the minimum of S_0.

Electronic dephasing and vibrational relaxation are then introduced via coupling to the environment, which is approximated as an assembly of harmonic oscillators with coupling strengths determined by the *spectral density*.

Fig 1: Open quantum system. An external laser field excites the system, which then dissipates energy into the bath degrees of freedom, involving both Markovian (system to bath) and non-Markovian (bath to system) information transfer.

Hierarchical Equations of Motion

$$J_n(\omega) = 2\eta_n \frac{\omega\Lambda_n}{\omega^2 + \Lambda_n^2}$$

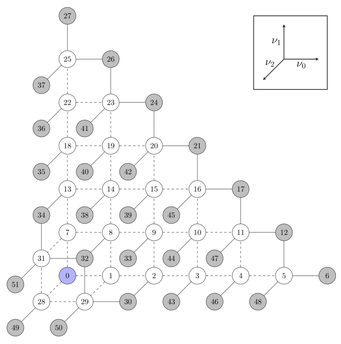

Using the Drude spectral density, $J_n(\omega)$, for an overdamped bath, we derive an hierarchy of equations of motion (HEOM).[4] Simultaneous propagation of a series of auxiliary density operators (ADO), $\rho_{\mathbf{j}}(t)$, accounts for non-Markovian memory effects which influence spectral broadening.[5]

$$\dot{\rho}_{\mathbf{j}}(t) = -\left(\frac{i}{\hbar}\mathsf{H}_{\mathrm{S}}^{\times} + \sum_{n=1}^{N}\sum_{k=0}^{M} j_{nk}\nu_{nk}\right)\rho_{\mathbf{j}}(t) - i\sum_{n=1}^{N}\sum_{k=0}^{M} j_{nk}\left(c_{nk}\mathsf{B}_n\rho_{j_{nk}^-}(t) - c_{nk}^*\rho_{j_{nk}^-}(t)\mathsf{B}_n\right)$$
$$-i\sum_{n=1}^{N}\sum_{k=0}^{M}\mathsf{B}_n^{\times}\rho_{j_{nk}^+}(t) - \sum_{n=1}^{N}\left(\frac{2\eta_n}{\hbar\beta\Lambda_n} - \eta_n\cot\left(\frac{\hbar\beta\Lambda_n}{2}\right) - \sum_{k=1}^{M}\frac{c_{nk}}{\nu_{nk}}\right)\mathsf{B}_n^{\times}\mathsf{B}_n^{\times}\rho_{\mathbf{j}}(t)$$

Fig 2: Hierarchy diagram showing connections between ADOs. Each axis is sealed with terminators (grey) and $\rho_{\mathbf{0}}$ is the reduced density matrix of the system, ρ_{S} (blue).

Termination Criterion

Markovian limit = ξ :

$$\frac{2(M+1)\pi}{\hbar\beta} > \xi \qquad \sum_{n=1}^{N}\sum_{k=0}^{M} j_{nk}\nu_{nk} > \xi$$

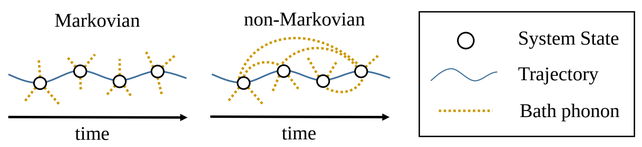

Fig 3: Markovian vs. non-Markovian dynamics. In Markovian, system-bath interactions occur at a constant rate, whilst in non-Markovian, previous interactions can feedback into the system some time later, requiring a *memory* of previous states, provided by the ADOs.

2D Electronic Spectroscopy

The interaction of three ultrafast laser pulses, separated by the coherence, τ, and population, T, times, generates a third order polarisation, $P^{(3)}(\tau,T,t)$, in the rephasing and non-rephasing directions.

Spectra are calculated in the impulsive limit from the molecular response function[5] and for finite fields using the equation of motion-phase matching approach (EOM-PMA).[3]

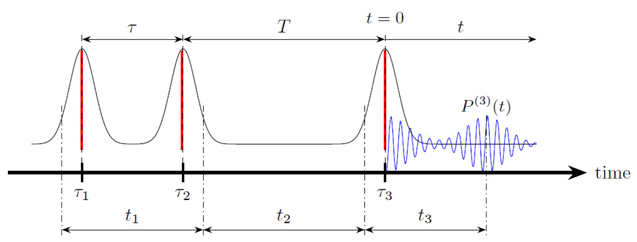

Fig 4: Pulse sequence and waiting times in 2D spectroscopy for impulsive (red) and finite (black) field envelopes.

a) Non-rephasing (real), T = 300 fs

b) Rephasing (real), T = 300 fs

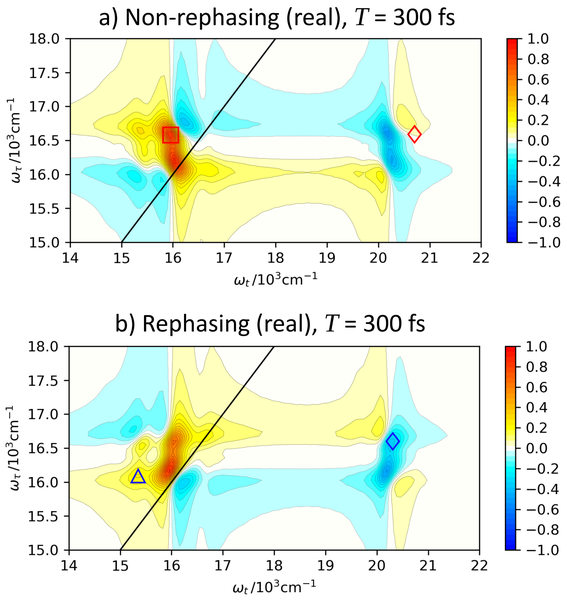

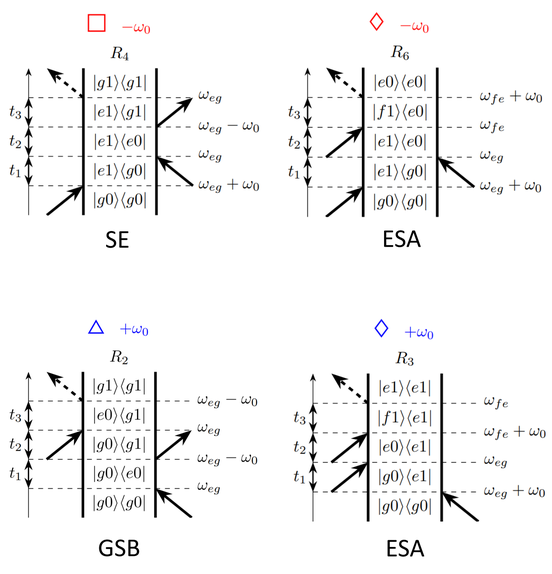

Fig 5: a) Non-rephasing and b) Rephasing half-broadband 2D electronic spectra at T = 300 fs for 585 cm^{-1} cresyl violet vibronic model. The locations of example double-sided Feynman diagrams are shown within the spectra where red (blue) indicates a negative (positive) vibrational coherence and the square, triangle or diamond correspond to stimulated emission (SE), ground state bleach (GSB) or excited state absorption (ESA) pathways, respectively.

Vibrational Coherence Beating Maps for 585 cm^{-1} Mode

The larger displacement between S_0 and S_1 for the 585 cm^{-1} mode[6] shows a clear vibronic progression in the absorption spectrum, with greatest intensity in the GSB/SE region of the beating maps.

Spectral filtering due to the finite pump spectrum obscures peaks with lower excitation frequency in good agreement with experimental beating maps.

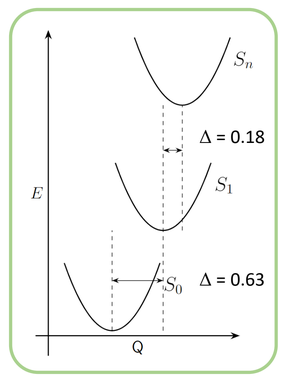

Fig 6: Potential energy surface along the 585 cm^{-1} mode coordinate, Q, showing greater displacement between S_0 and S_1 than S_1 and S_n.

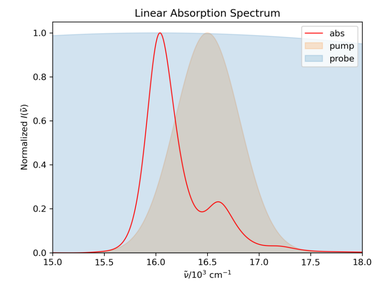

Fig 7: Linear absorption spectrum (red) for the 585 cm^{-1} mode model with pump and probe spectra used for half-broadband 2DES overlaid.

a) Peak Location Key Diagram

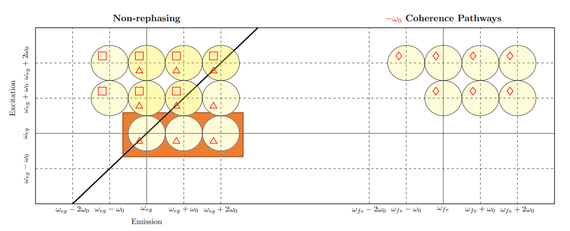

b) Impulsive limit

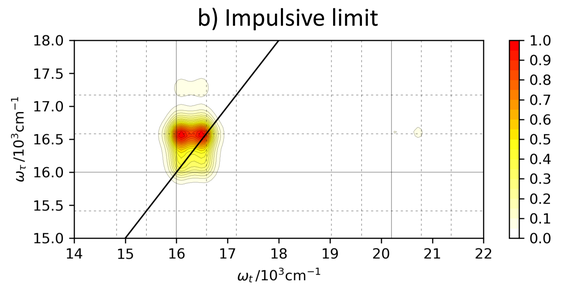

c) Experimental

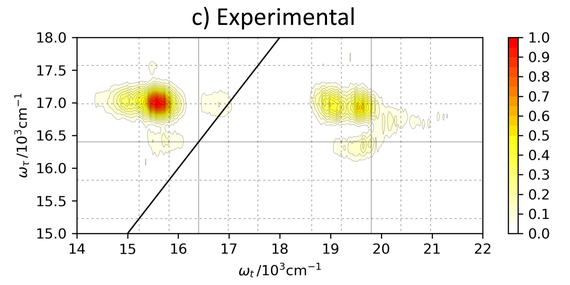

d) Finite pump spectrum

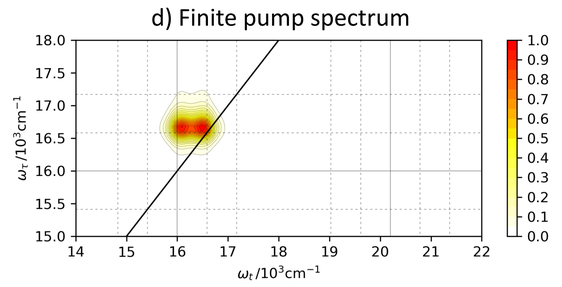

Fig 8: a) Key diagram showing predicted location of peaks in a negative non-rephasing vibrational beating map, with pathways filtered by the finite pump spectrum in figure 7 highlighted in orange. Non-rephasing ω_T = -585 cm^{-1} beating maps: b) calculated in the impulsive limit (broadband), d) calculated including the finite pump spectrum (half-broadband) and c) measured experimentally.

Vibrational Coherence Beating Maps for 350 cm^{-1} Mode

The larger displacement between S_1 and S_n for the 350 cm^{-1} mode shows the greatest intensity in the ESA region of the beating maps, as seen in the experimental results.

However, significant GSB/SE intensity remains in the calculated beating maps and the lower excitation frequency peak in the experimental results is unassigned using the current model.

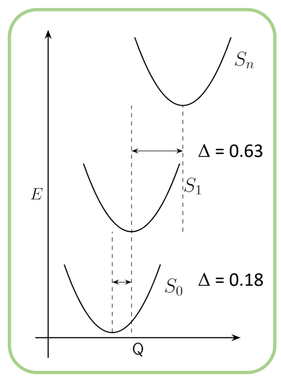

Fig 9: Potential energy surface along the 350 cm^{-1} mode coordinate, Q, showing greater displacement between S_1 and S_n than S_0 and S_1.

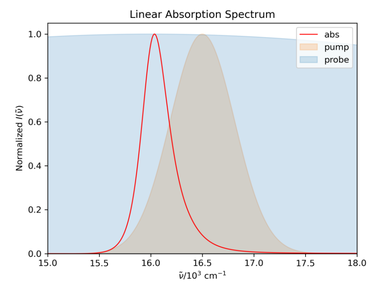

Fig 10: Linear absorption spectrum (red) for the 350 cm^{-1} mode model with pump and probe spectra used for half-broadband 2DES overlaid.

a) Peak Location Key Diagram

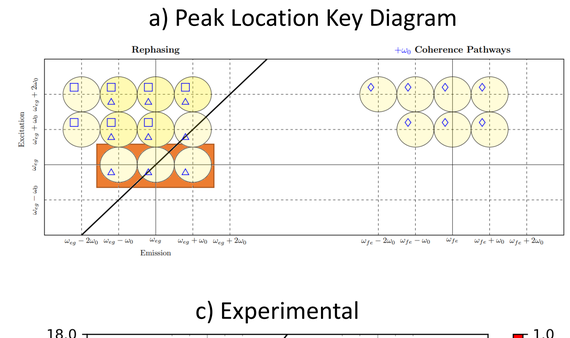

b) Impulsive limit

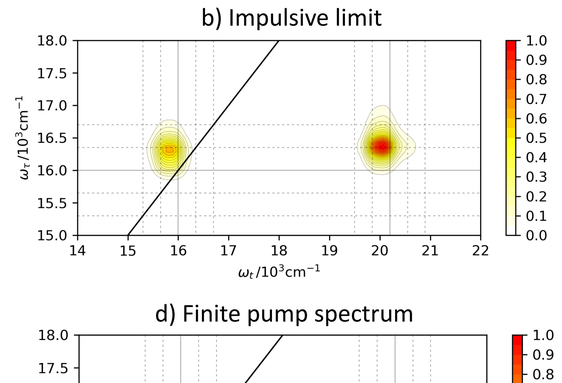

c) Experimental

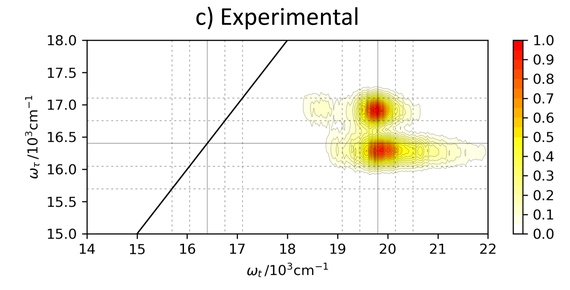

d) Finite pump spectrum

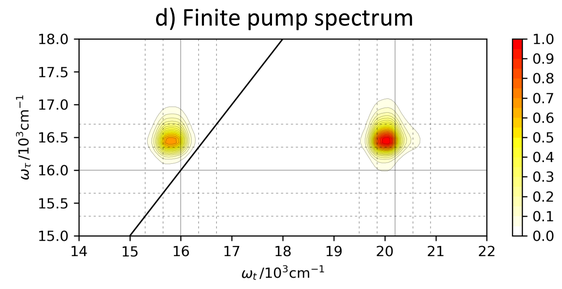

Fig 11: a) Key diagram showing predicted location of peaks in a positive rephasing vibrational beating map, with pathways filtered by the finite pump spectrum in figure 10 highlighted in orange. Rephasing ω_T = +350 cm^{-1} beating maps: b) calculated in the impulsive limit (broadband), d) calculated including the finite pump spectrum (half-broadband) and c) measured experimentally.

Conclusion

Separate vibronic models for the 350 cm^{-1} and 585 cm^{-1} modes of cresyl violet demonstrated the filtering of lower excitation frequency peaks in half-broadband 2DES beating maps due to the finite pump spectrum compared with broadband 2DES in the impulsive limit. The relative intensity of the GSB/SE and ESA peaks was also shown to be a result of the relative displacement of the S_1 and S_n excited states with respect to S_0. Future work includes extension to a multimode vibronic model, which introduces new pathways involving both modes, in combination with the new broadband 2DES experiment under development at RAL.

References

1) C.C. Jumper, S. Rafiq, S. Wang, and G.D. Scholes, Curr. Opin. Chem. Biol. **47**, 39 (2018).
2) S. Biswas, J. Kim, X. Zhang, and G.D. Scholes, Chem. Rev. **122**, 4257 (2022).
3) D. Green, F. V. A. Camargo, I.A. Heisler, A.G. Dijkstra, and G.A. Jones, J. Phys. Chem. A **122**, 6206 (2018).
4) Y. Tanimura, J. Chem. Phys. **153**, 020901 (2020).
5) D. Green, B.S. Humphries, A.G. Dijkstra, and G.A. Jones, J. Chem. Phys. **151**, 174112 (2019).
6) G. Batignani, C. Sansone, C. Ferrante, G. Fumero, S. Mukamel, and T. Scopigno, J. Phys. Chem. Lett. **12**, 9239 (2021).

Acknowledgements

This study was supported by the Engineering and Physical Sciences Research Council under Awards No. EP/V00817X/1. Calculations presented in this paper were carried out on the High Performance Computing Cluster supported by the Research and Specialist Computing Support service at the University of East Anglia.